Available online at www.sciencedirect.com
ScienceDirect
ELSEVIER
Palaeogeography, Palaeoclimatology, Palaeoecology 244 (2007) 126–141
PALAEO
www.elsevier.com/locate/palaeo

End-Triassic calcification crisis and blooms of organic-walled 'disaster species'

B. van de Schootbrugge [a,*], F. Tremolada [b], Y. Rosenthal [a,b], T.R. Bailey [c], S. Feist-Burkhardt [d], H. Brinkhuis [e], J. Pross [f], D.V. Kent [b], P.G. Falkowski [a,b]

[a] *Institute of Marine and Coastal Sciences, Rutgers, the State University of New Jersey, 71 Dudley Road, 08901-NJ, USA*
[b] *Department of Geological Sciences, Rutgers, the State University of New Jersey, 610 Taylor Road, Piscataway NJ 08854, USA*
[c] *National Museums and Galleries of Wales, Cathays Park, CF10 3NP Cardiff, Wales, UK*
[d] *Palaeontology Department, Natural History Museum of London, Cromwell Road, London, England, UK*
[e] *Laboratory of Palaeobotany and Palynology, Utrecht University, Budapestlaan 4, 3584, CD Utrecht, The Netherlands*
[f] *Institute for Earth Sciences, Johann-Wolfgang Goethe University Frankfurt, Senckenberganlage 32-34, D-60054 Germany*

Accepted 20 June 2006

Abstract

The Triassic–Jurassic (T–J) mass-extinction event is marked by isotope anomalies in organic ($\delta^{13}C_{org}$) and carbonate carbon ($\delta^{13}C_{carb}$) reservoirs. These have been attributed to a (rapid) 4-fold rise in pCO_2 as a result of massive flood basalt volcanism and/or methane hydrate dissociation. Here we examine the response of marine photosynthetic phytoplankton to the proposed perturbation in the carbon cycle. Our high-resolution micropalaeontological analysis of T–J boundary beds at St Audrie's Bay in Somerset, UK, provides evidence for a bio-calcification crisis that is characterized by (1) extinction and malformation in calcareous nannoplankton and (2) contemporaneous blooms of organic-walled, green algal 'disaster' species which comprise in one case >70% of the total palynomorph fraction. Blooms of prasinophytes and acritarchs occur at the onset and in association with a prominent negative shift in $\delta^{13}C_{org}$ values close to the first appearance of the Early Jurassic ammonite *Psiloceras planorbis*. Across the same interval we obtained palaeotemperature and palaeosalinity estimates from oyster low-Mg calcite based on Mg/Ca, Sr/Ca and $\delta^{18}O$ records. The results of our palynological and geochemical analyses strongly suggest that shallow marine basins in NW Europe during this period became salinity stratified, inducing anoxic conditions. The T–J boundary event shows similarities with the Permian–Triassic (P–T) mass-extinction event, which was also marked by extensive flood basalt volcanism, negative excursions in carbon isotope records, a bio-calcification crisis, the development of shallow-marine anoxia and mass abundances of acritarchs in the Early Triassic. This leads us to suggest that the proliferation of green algal phytoplankton may be symptomatic of elevated carbon dioxide levels in the atmosphere and oceans during mass-extinction events.

Keywords: Triassic–Jurassic boundary; Carbon cycle; Phytoplankton evolution; Stable isotopes; Trace elements

1. Introduction

The Triassic–Jurassic (T–J) boundary mass-extinction (~200.5 Ma ago) has long been recognized as one of five major Phanerozoic extinction events (Newell, 1963; Tanner et al., 2004). At that time ~80% of all species went extinct

* Corresponding author. Present address: Micropaleontology and Palaeoceanography Group, Institute of Geology and Paleontology, Johann Wolfgang Goethe University Frankfurt, Senckenberganlage 32-34, D-60054 Frankfurt, Germany. Tel.: +49 69 798 22769; fax: +49 69 798 22958.
E-mail address: van.de.Schootbrugge@em.uni-frankfurt.de (B. van de Schootbrugge).

0031-0182/$ - see front matter © 2007 Published by Elsevier B.V.
doi:10.1016/j.palaeo.2006.06.026

(Sepkoski, 1996) and marine ecosystems were especially perturbed, with high extinction rates among ammonites and conodonts. Profound changes in the terrestrial biosphere were less marked, but apparently important enough to allow dinosaurs to evolve rapidly during the Jurassic recovery phase (Olsen et al., 2002). Various, non-exclusive scenarios have been proposed to explain the loss of terrestrial and marine bio-diversity, including a bolide impact (Olsen et al., 2002), sea level change (Hallam, 1997; Hallam and Wignall, 1997a), gas hydrate dissociation (Beerling and Berner, 2002), and massive flood basalt volcanism (Marzoli et al., 1999; Hesselbo et al., 2002).

A carbon isotope record derived from bulk organic carbon ($\delta^{13}C_{org}$; Hesselbo et al., 2002, 2004) from the St Audrie's Bay section (UK) shows a double (*initial* and *main*; Fig. 1) negative shift in carbon isotopes just prior to the last occurrence of Triassic conodonts and preceding the first appearance of Jurassic ammonites, respectively. It has been suggested that the carbon isotope record signals a rapid rise in atmospheric pCO_2. Leaf stomatal indices have been taken as evidence for a possible 4-fold increase in pCO_2 across the T–J boundary (McElwain et al., 1999). Negative carbon isotope excursions that occur simultaneously in bulk organic carbon (Nevada, USA; Guex et al., 2003, 2004), wood remains (Greenland; McElwain et al., 1999) and marine carbonates (e.g. in British Columbia, Canada; Ward et al., 2001, 2004) indicate that the entire carbon reservoir (marine, terrestrial and atmospheric) was affected. The emplacement and degassing of the Central Atlantic Magmatic Province (CAMP), one of the largest continental flood basalt provinces in the world (covering $7*10^6$ km^2 and with a volume of $2–4*10^6$ km^3; Marzoli et al., 1999) has been suggested as the primary source of CO_2 (Hesselbo et al., 2002), with an estimated release of 8000–9000 Gt in addition to the dissociation of 5000 Gt of methane (Beerling and Berner, 2002). Galli et al. (2005) proposed that Late Triassic carbonate platforms along the southern Tethyan margin drowned as a consequence of decreased over-saturation. A Triassic–Jurassic boundary 'bio-calcification crisis' is also expressed by an Early Jurassic (Hettangian–Sinemurian) coral reef gap, lasting possibly up to 8 Ma (Stanley, 2001). Moreover, other calcareous organisms, such as bivalves, appear to have experienced severe problems with calcification and changed their mineralogy from aragonite to calcite (Hautmann, 2004).

Here we report on the response of marine organic-walled and calcareous phytoplankton to the observed Triassic–Jurassic carbon cycle perturbation from an interval across the 'main' negative C-isotope excursion in St Audrie's Bay. The taxonomic composition of the phytoplankton assemblage potentially records changes in temperature, salinity, nutrients and pCO_2 (Tappan, 1980). To assess the influence of temperature and salinity on phytoplankton abundance, we include $\delta^{13}C$ and $\delta^{18}O$ and Mg/Ca and Sr/Ca data obtained from biogenic (oyster) calcite from the same section. Our results indicate that calcareous phytoplankton suffered a setback while organic-walled phytoplankton, belonging to green algal classes, apparently thrived during the main carbon cycle perturbation. We discuss a scenario in which CO_2-induced greenhouse warming led to changes in ocean chemistry and circulation, such as altered alkalinity and stratification.

2. Materials and methods

Palynological processing was performed at the Natural History Museum of London (UK) using standard acid treatment (alternating steps with HCl and HF) and sieving at 15 μm. Because of generally elevated amounts of amorphous organic matter (AOM), oxidative maceration ($KClO_3$ and 65% HNO_3) and bleaching, followed by staining with Bismark Brown, proved necessary for all samples. Initially 300 palynomorphs were counted per slide using a transmitted-light microscope at a 630× magnification. Subsequently, the slides were entirely scanned for less common elements and photographs were taken. Marine phytoplankton were determined to the species level, while terrestrial palynomorphs were grouped and counted in the categories 'pollen' and 'spores'. *Classopollis* spp. was counted separately, as this taxon may be useful for palaeo-environmental reconstructions. Additionally, the spore taxon *Kraeuselisporites reissingeri* was counted separately because of its stratigraphic value. In sample SAB-13, the organic matter was too severely degraded to allow for meaningful counts and this sample was excluded from further analysis.

Calcareous nannofossils were analyzed using the standard smear slide preparation technique (Bown and Young, 1998). In contrast to the palynological data, calcareous nannofossils were only studied qualitatively. Calcareous nannofossils are extremely rare across the Triassic–Jurassic boundary for reasons further discussed below.

Samples of the oyster *Liostrea hisingeri* were collected along with bulk rock samples for micropalaeontological analysis from the Triassic–Jurassic boundary beds at St Audrie's Bay. Height of the samples in the stratigraphic section are reported relative to the base of the Williton Member to allow comparison with the organic carbon isotope data of Hesselbo et al. (2002, 2004), which were obtained from the same locality. Where possible, several individual oysters were collected from the same stratigraphic level. After separation of fragments of oyster

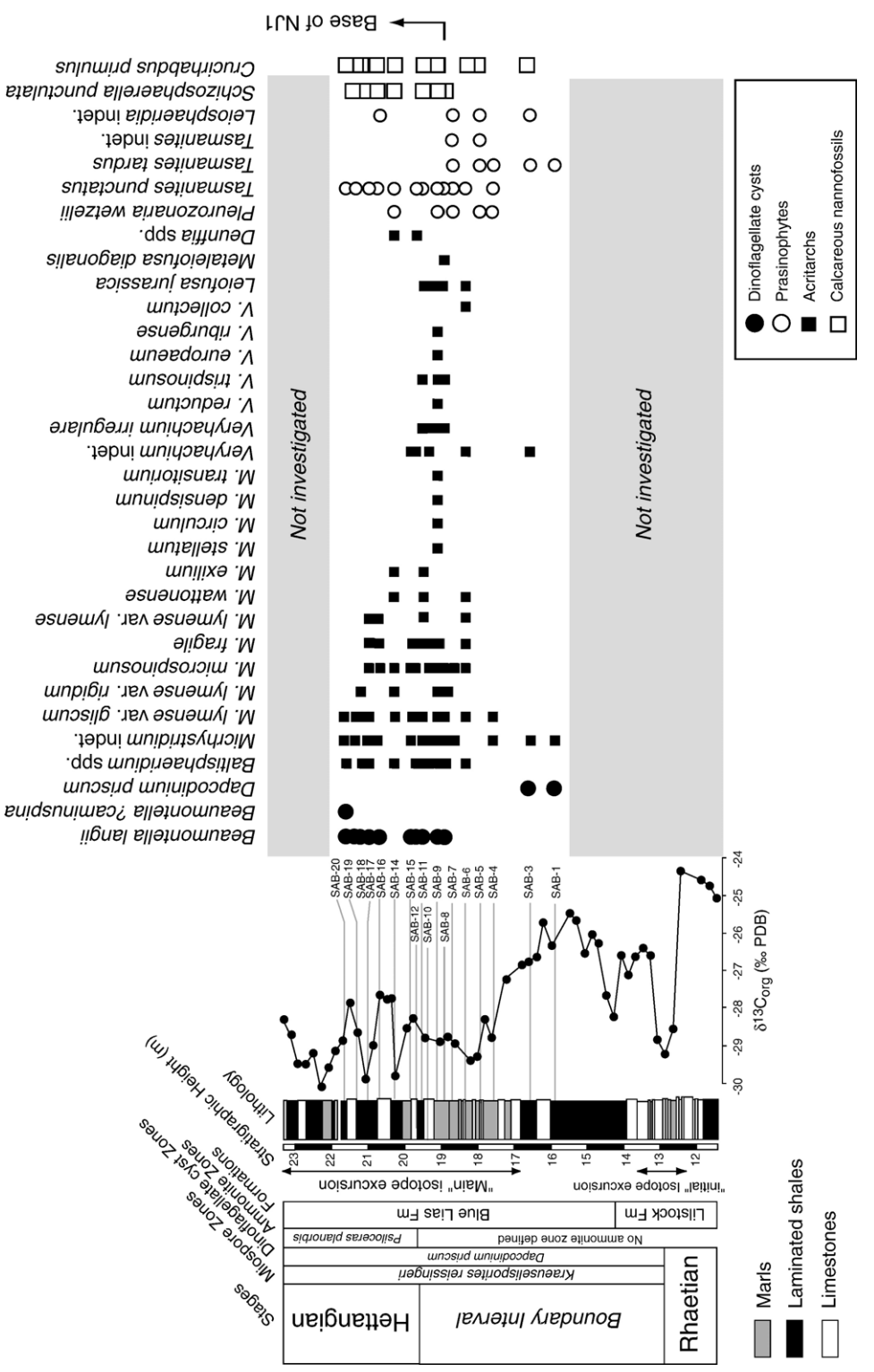

Fig. 1. Range chart of identified of organic-walled phytoplankton and *Schizosphaerella punctulata*, showing the incidence of blooms of prasinophytes and acritarchs at the onset of and during the main negative C-isotope excursion in St Audrie's Bay section. Lithology and carbon isotope data are after Hesselbo et al. (2002, 2004). Note that the sample numbers are not in sequential order and that the labels are different from those used for oyster geochemistry. Sample SAB-14 is stratigraphically higher than sample SAB-15.

Table 1
Palynological data (absolute counts) for St Audrie's Bay section

	Pollen			Spores			Dinocysts			Acritarchs																						Prasinophytes						
Sample #	Pollen indet	*Classopollis* spp.	*Classopollis* tetrads	*Trilete spores* indet	*Kraeuselisporites reissingeri* tetrads	*Kraeuselisporites reissingeri*	*Beaumontella langii*	*Beaumontella caminuspina*	*Dapcodinium priscum*	*Baltisphaeridium* spp.	*Micrhystridium* indet	*Micrhystridium lymense* var. *gliscum*	*Micrhystridium lymense* var. *rigidum*	*Micrhystridium microspinosum*	*Micrhystridium fragile*	*Micrhystridium lymense* var. *Lymense*	*Micrhystridium wattonense*	*Micrhystridium exilium*	*Micrhystridium stellatum*	*Micrhystridium circulum*	*Micrhystridium densispinum*	*Micrhystridium transitorium*	Veryhachium indet	*Veyhachium irregulare*	*Veyhachium reductum*	*Verylachium trispinosum*	*Verylachium europaeum*	*Verylachium riburgense*	*Verylachium collectum*	*Leiofusa jurassica*	*Metaleiofusa diagonalis*	*Pleurozonaria wetzelii*	*Tasmanites punctatus*	*Tasmanites tardus*	*Tasmanites* indet	*Leiosphaeridia* spp.	*Deunffia* sp.	Foraminifera innerwall linings
SAB-1	229	38	1						51		3																						13					
SAB-3	244	23							12		1												1										10		9			
SAB-4	83	86		11							7	1																		4	6	107					
SAB-5	183	84		24																										2		4	1	2			
SAB-6	87	110	1	3	1	1				5		72		1	3	3	6						1						1	4		3					
SAB-7	33	3		6							4			202																24	20	7	5	9			
SAB-8	10	64	7	2			3			10	4	36	1	80										3		8				64	1		7				
SAB-9	43	45	1	1			6			4	25	20	12	60	2				1	1	1	4		9	10	9	1	1		31		2	11				
SAB-10	73	130	2	5						10	11	38		17	3								3	1					7							
SAB-11	149	35	7	4			3			18	4	58			5	3	4	2					1	1		1			2			3				
SAB-12	44	193	4		1	1	2			20		14		8									5									7			1	
SAB-14	90	112	14	2						26		23	15	8			2	1												3	3				1	
SAB-15	81	135	7	4	2	11	16				3	25		3	1																6					6
SAB-16	82	181	6	2			1			6	1			6		1															13			1		
SAB-17	6	234	20				1			6	6	16		7	1	2															1					
SAB-18	10	184	24				1			39	7	22	13																							
SAB-19	50	202	2	5		21	2				10	1																			7					
SAB-20	49	190	14	2	4	10	5	1		4	13	6																			2					

calcite from the rock matrix, outer layers were removed and powdered samples were generated using a hand-held dental drill.

Calcite powders were homogenized and split for trace element and stable isotopic analyses. Samples for stable isotope analyses were reacted with 100%

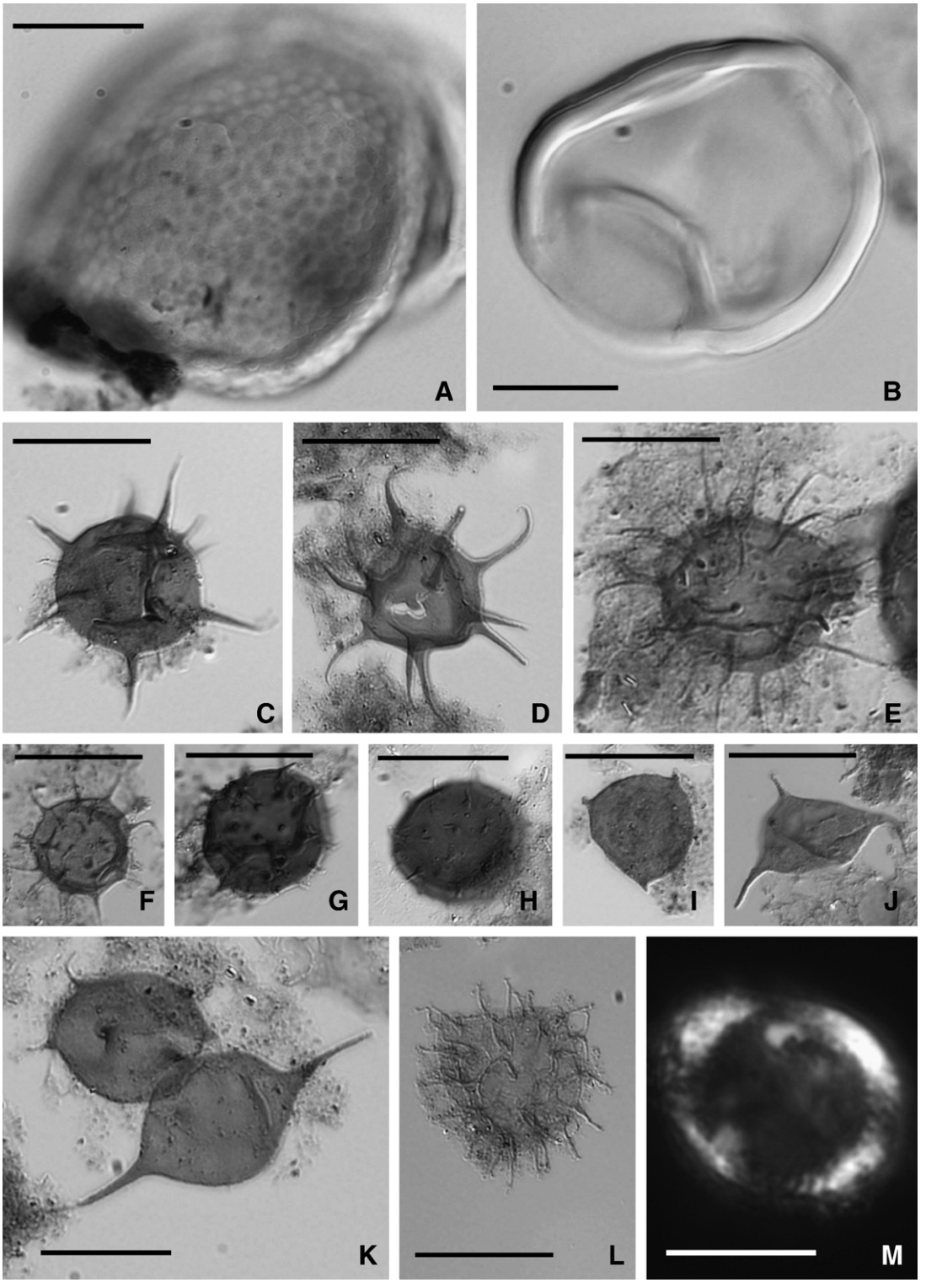

orthophosphoric acid at 90 °C using a Multi-prep peripheral device and analysed with an Optima mass spectrometer at Rutgers University. Repeat analysis of NBS19 yielded precision better than ±0.06‰ for $\delta^{13}C$ and better than ±0.08‰ for $\delta^{18}O$. Isotopic values are reported relative to ‰ PDB.

Samples for trace element analysis were dissolved in 0.065N HNO_3, and diluted with 0.5 N HNO_3 to ~4 mM Ca concentration. Acids were prepared using ultrapure SEASTAR® 16 N HNO_3 and ddH_2O. Mg/Ca and Sr/Ca were measured using a Finnigan MAT Element Sector Field Inductively Coupled Plasma Mass Spectrometer (ICP-MS) operated in low resolution ($m/\Delta m = 300$) following the method outlined in Rosenthal et al. (1999) and modified by Lear et al. (2002). During the study period the analytical precision as determined by replicate analysis of consistency standards was better than 1% rsd (1σ) for Mg/Ca (7.5 mmol mol^{-1}) and Sr/Ca (1.8 mmol mol^{-1}). Measurements of Mn/Ca, Fe/Ca and Al/Ca were used to monitor for diagenesis and contamination from silicate phases; samples in which either of these ratios exceeded the levels of Mn/Ca over 200 μmol mol^{-1}, Fe/Ca over 500 μmol mol^{-1}, or Al/Ca over 80 μmol mol^{-1} were discarded.

3. Results

3.1. Micropaleontology

Our results indicate dramatic changes in phytoplankton assemblages across the main C-isotope excursion. These include a decline in calcareous nannofossil species and concomitant blooms in organic-walled phytoplankton (Fig. 1, Table 1). We find rare and poorly preserved calcareous nannofossils in this sequence. The only calcareous species preserved across the T–J boundary were *Crucirhabdus primulus* and *Schizosphaerella punctulata*. In St Audrie's Bay, the first appearance of *S. punctulata* in sample SAB-8 (Figs. 1 and 2) slightly predates the base of the *Psiloceras planorbis* ammonite zone and correlates with the onset of the main negative excursion in $\delta^{13}C_{org}$ values documented by Hesselbo et al. (2002, 2004). The results presented here confirm the initial report of Hamilton (1982) who observed *S. punctulata* in the St Audrie's Bay section.

In lieu of the calcareous phytoplankton we observe a rise in organic-walled taxa, mainly composed of acritarchs and prasinophytes. Preceding the main C-isotope excursion (Fig. 1; Table 1) we find a typical late Rhaetian assemblage characterized by high abundances of the dinoflagellate cyst *Dapcodinium priscum* (sample SAB-1). With the onset of the main C-isotope excursion, prasinophyte phycomata assignable to *Tasmanites* start to dominate and dinoflagellate cysts are absent, while acritarchs tend to be rare. Sample SAB-4 contains abundant prasinophyte phycomata assignable to *Tasmanites tardus*. This acme is followed by an almost monospecific occurrence of the acritarch *Micrhystridium microspinosum* in sample SAB-7, which constitutes more than 70% of the total palynomorph assemblage (Fig. 3H). Sample SAB-8 is dominated by the acritarch *Leiofusa jurassica* (making up 20% of the total palynomorph assemblage). In these samples we also found a low-abundance, high-diversity, assemblage of prasinophytes, including the distinctive *Pleurozonaria wetzelii*. Coinciding with some of the most negative C-isotope values, sample SAB-9 shows a remarkable diversity in acritarch taxa (15 different species and varieties) with *Veryhachium trispinosum*, *M. microspinosum*, *Baltisphaeridium* spp. and *L. jurassica* as the most abundant forms (Fig. 2). Sample SAB-9 also shows the presence of the dinoflagellate cyst *Beaumontella langii*. Acritarch diversity declines again in sample SAB-11 with *Micrhystridium lymense* var. *gliscum* becoming the most dominant form. However, overall abundance of acritarchs and prasinophytes decreases and remains low from this point on.

3.2. Geochemistry

Our combined $\delta^{13}C$, $\delta^{18}O$, Mg/Ca and Sr/Ca data obtained from oyster (low-magnesium) calcite show intriguing co-varying trends (Fig. 3B–E; Table 2). The oyster carbon isotope values decrease by 2.2‰ during the main C-isotope excursion. This decrease is smaller than the 4‰ negative change observed in the $\delta^{13}C_{org}$ record across the same interval. The oyster oxygen isotope record shows a sharp decrease of 2.5‰ that is mirrored by an increase in Mg/Ca of ~4.0 mmol mol^{-1} and Sr/Ca of 0.12 mmol mol^{-1}. Carbon and oxygen isotope values from bulk carbonate samples reported by

Fig. 2. For all palynomorphs scale bars represent 20 μm, except for *Schizosphaerella punctulata* (M) where the scale bar is 5 μm. (A) *Pleurozonaria wetzelii*, sample SAB-7; (B) *Tasmanites tardus*, sample SAB-4; (C) *Micrhystridium lymense* var. *gliscum*, sample SAB-9; (D) *M. fragile*, sample SAB-9; (E) *Baltisphaeridium* spp., sample SAB-9; (F) *M. lymense* var. *rigidum*, sample SAB-9; (G) *M. microspinosum*, sample SAB-9; (H) *M. microspinosum*, sample SAB-9, note the variability in number of spines compared to the previous specimen. (I) *Veryhachium reductum*, sample SAB-9; (J) *Veryhachium trispinosum*, sample SAB-9; (K) Lower right: *Leiofusa jurassica*. Upper left: *Veryhachium irregulare*, sample SAB-9; (L) *Beaumontella langii*, sample SAB-9; (M) *Schizosphaerella punctulata*, sample SAB-8.

Hallam (1994) are on average 5‰ more negative, with some values as low as −11‰ for $\delta^{18}O$. Hence, we suggest that oyster calcite from St Audrie's Bay has undergone less diagenetic overprint than the bulk carbonate matrix. However, are these oysters pristine, i.e. can they be used to document changes in Early Mesozoic palaeotemperature and palaeosalinity?

To assess oyster calcite for possible diagenetic alteration, trace element contents (Fe, Mn, Al) were determined. Measurements with Mn/Ca in excess of 200 μmol mol^{-1} (~110 ppm Mn) or Fe/Ca larger than 500 μmol mol^{-1} (~280 ppm Fe) were discarded. Such high concentrations have commonly been used as cut-off limits (e.g. Brand and Veizer, 1980). Samples with high Al content, >60 μmol mol^{-1} (~16.2 ppm), were also discarded to avoid contamination from non-carbonate minerals (e.g. Barker et al., 2003). Nine measurements were discarded from a total of 55 analyses (see Table 2b). There is no consensus of opinion on absolute values for such trace element rejection criteria, due to the large range of concentrations seen in modern biogenic carbonates (e.g. Morrison and Brand, 1986). The rejection criteria used here were chosen as they remove all correlation between the elemental ratio used as diagenetic indicators (Mn/Ca, Fe/Ca, Al/Ca) and stable isotope or elemental ratios of interest on cross-plots (Fig. 4). The absence of any trends on the cross-plots after data rejection suggests that the screened data represent well-preserved oyster calcite. In addition, our screened data are comparable to the range of concentrations seen in modern oysters (*cf.* Table 3).

To test the extent of intra-shell variability in isotopic and trace element content, two entire oyster valves were serially sampled from the umbo to the margin (Table 4). The intra-shell variability does not exceed observed differences between individual shells from the same stratigraphic level. The intra-shell standard error (%) calculated from multiple analyses of a single shell is equivalent to the inter-shell standard error obtained from the analyses of several different shells from the same stratigraphic level. The means of both the intra-shell and inter-shell analysis are the same, given these standard errors. Therefore we have not distinguished between serially sampled oysters and individual oysters from the same horizon in our stratigraphic plots (Fig. 3B–E).

4. Discussion

4.1. Biostratigraphy

The St Audrie's Bay succession in Somerset, UK, is a candidate for a Global Stratotype Section and Point (GSSP), and is considered to be one of the more complete shallow marine sections in the world straddling the T–J boundary (Warrington et al., 1994). In the St Audrie's Bay section, the T–J boundary has conventionally been placed at the lowest occurrence of the Hettangian ammonite *Psiloceras planorbis* by Warrington et al. (1994). Various other authors favour different stratigraphic levels; Hesselbo et al. (2002, 2004) prefer a position close to the initial C-isotope excursion in the Lilstock Formation (Fig. 1). Uncertainty regarding the exact position of the T–J boundary in St Audrie's Bay pertains to several independent stratigraphic methods. A recently updated magnetostratigraphic zonation for the St Audrie's Bay section by Hounslow et al. (2004) does not show an obvious correlation between either Rhaetian magneto-zone SA5n.2r or Hettangian magneto-zone SA5r of the St Audrie's Bay section and magneto-zone E23r in the Newark Basin, which is of latest Rhaetian age. Other geochemical proxies for environmental change, such as the Osmium isotope ($^{187}Os/^{186}Os$) record and Rhenium (Re) concentration (Cohen and Coe, 2002), show anomalies close to the base of the *P. planorbis* ammonite Zone in conjunction with the main C-isotope excursion. However, anomalous values also occur in association with the initial C-isotope excursion. Finally, changes in pollen and spore assemblages appear gradual rather than abrupt, and many marker species, such as *Kraeuselisporites reissingeri*, have a Late Triassic to Early Jurassic range.

Our acritarch and prasinophyte acmes also occur close to the base of the *Psiloceras planorbis* Zone and may therefore have a stratigraphic value. However, until now, reports on acritarch spikes in association with the T–J boundary have been limited. The sole mention of abundant prasinophytes (*Tasmanites, Pleurozonaria and Cymatiosphaera*) and acritarchs (*Leiofusa jurassica*) in direct association with the transition from the Rhaetian into the Hettangian, stems from a low resolution study (3 samples) of a temporary outcrop in northern Germany (Sehnde Mittellandkanal, Lower Saxony: Beutler et al., 1996). Previous studies on the palynology of the St Audrie's Bay section by Orbell (1973) and Warrington (as reported in Hounslow et al., 2004) appear to have missed the acritarch and prasinophyte acme, possibly due to a lower sampling resolution or a different strategy in sample processing. However, Hounslow et al. (2004) mention that acritarchs appear to increase in diversity in the basal part of the Blue Lias Group. Further down, the Rhaetian is not marked by any mass-abundances of acritarchs or prasinophytes, even though *Micrhystridium*, *Veryhachium* and a handful of prasinophyte species are present throughout the Late Triassic (Courtinat et al., 1998). Other organic-walled taxa, such as the cyst-producing dinoflagellates *Rhaetogonyaulax rhaetica* and *Dapcodinium*

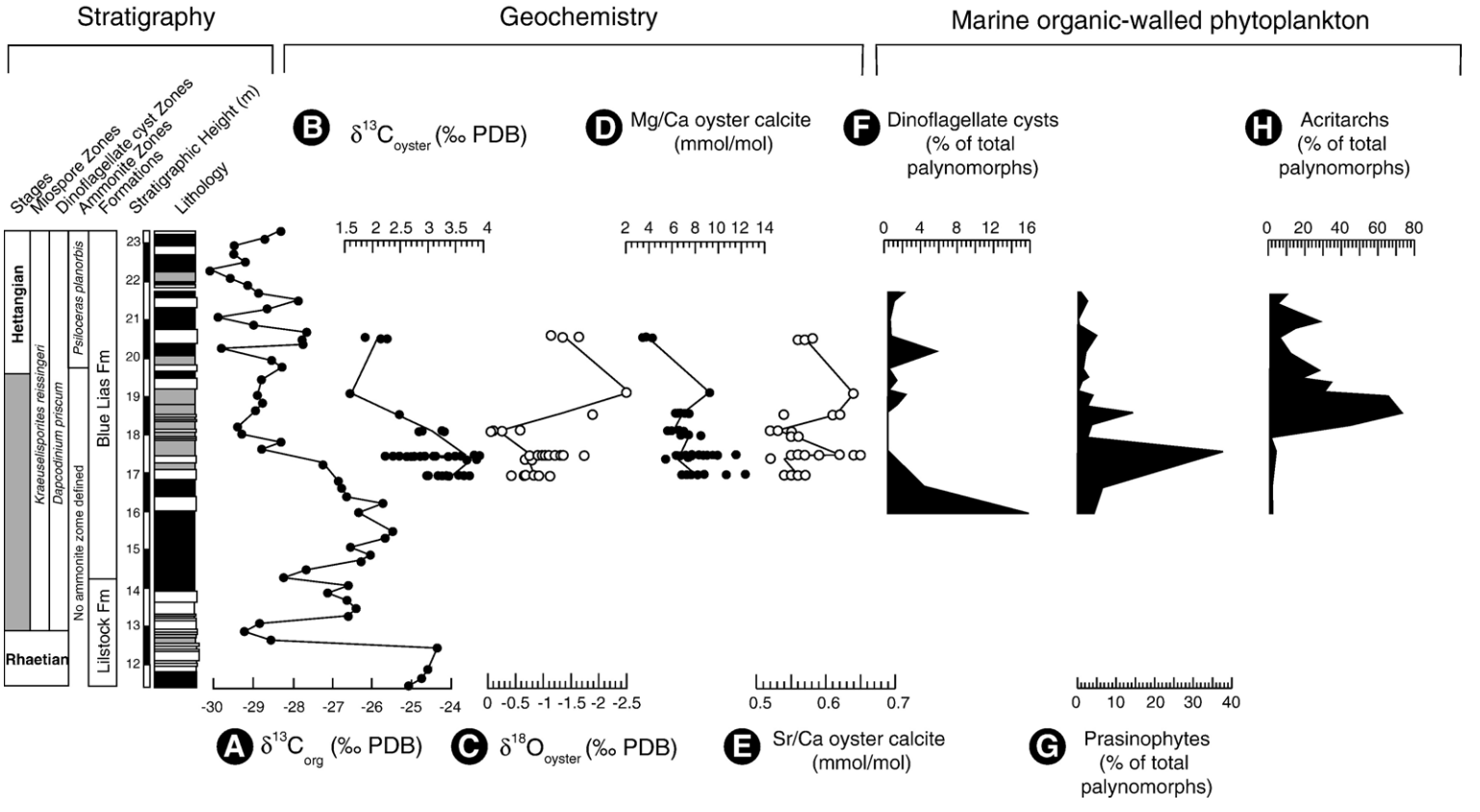

Fig. 3. Geochemical results from the oyster *Liostrea hisingeri* from the St Audrie's Bay section compared with percentage plots of marine phytoplankton abundance. The geochemical plots have 20% weighted average curve fits to highlight changes in the various proxies. (A) Stratigraphy, lithology and carbon isotope record ($\delta^{13}C_{org}$ in ‰ PDB) for bulk organic matter from Hesselbo et al. (2002). (B) Carbon isotope record for oysters ($\delta^{13}C_{oyster}$ in ‰ PDB; this study). (C) Oxygen isotope record for oysters ($\delta^{18}O_{oyster}$ in ‰ PDB; this study). (D) Mg/Ca record from oyster calcite (mmol mol^{-1}; this study). (E) Sr/Ca record from oyster calcite (mmol mol^{-1}; this study). (F) Dinoflagellate cyst abundance as a percentage of the total palynomorph fraction. (G) Prasinophyte phycomata abundance as a percentage of the total palynomorph fraction. (H) Acritarch abundance as a percentage of the total palynomorph fraction.

Table 2
(A) Geochemical data from diagenetically unaltered goysters. (B) Data from diagenetically altered oysters

Sample #	Height	δ^{13}X	2se	δ^{18}O	2se	Mg/Ca	2se	Sr/Ca	2se	Mn/Ca	2se	Fe/Ca	2se	Al/Ca	2se
	m	*permil*		*permil*		*mmol/mol*		*mmol/mol*		*μmol/mol*		*μmol/mol*		*μmol/mol*	
(A) Geochemical data from oyster *Liostrea hisingeri* — unaltered															
SAB03-2	20.59	1.87		−1.14		3.68		0.58		104.06		193.86		12.07	
SAB03-3	20.55	2.15		−1.64		4.27		0.57		113.80		156.02		13.96	
SAB03-3C	20.55	2.26		−1.35		3.59		0.56		82.10		118.20		21.69	
sab03-5	19.11	1.60		−2.47		9.23		0.64		105.73		95.46		17.03	
sab03-6a	18.56	2.49		−1.88		7.44		0.54		72.30		134.48		2.45	
sab03-7-1	18.55	na		na		7.07	0.39	0.61	0.01	134.29	55.23	165.23	59.36	33.84	27.07
sab03-7-2	18.55	na		na		6.68	0.39	0.62	0.01	71.49	55.23	206.17	59.36	55.27	27.07
sab03-7-3	18.55	na		na		6.39	0.39	0.61	0.01	40.40	55.23	104.03	59.36	8.45	27.07
SAB03-8	18.13	2.89		−0.57		6.61		0.52		47.17		85.51		36.82	
SAB03-8A	18.13	3.26		−0.09		5.89		0.53		46.31		139.60		8.26	
SAB03-9A	18.11	3.29		−0.25		5.59		0.55		44.84		135.11		21.08	
SAB03-9B	18.11	2.83		−0.07		7.01		0.53		59.09		166.63		30.87	
sab03-10	17.99	na		na		7.25		0.55		18.57		31.72		4.98	
sab03-11a	17.98	na		na		6.85		0.55		25.09		51.21		16.78	
sab03-11b	17.98	na		na		8.51		0.56		44.45		62.75		16.35	
sab03-13-1	17.48	na		na		6.65	1.38	0.59	0.02	64.24	7.38	34.45	57.89	5.37	6.85
sab03-13-2	17.48	na		na		6.49	1.38	0.62	0.02	58.64	7.38	234.63	57.89	12.12	6.85
sab03-13-3	17.48	na		na		6.33	1.38	0.65	0.02	44.16	7.38	56.87	57.89	12.32	6.85
sab03-13-4	17.48	3.92	0.25	−0.75	0.08	6.54	1.38	0.62	0.02	41.13	7.38	56.47	57.89	29.56	6.85
sab03-13-5	17.48	3.84	0.25	−0.74	0.08	7.24	1.38	0.64	0.02	43.73	7.38	25.16	57.89	8.86	6.85
sab03-13-6	17.48	3.59	0.25	−0.75	0.08	7.19	1.38	0.59	0.02	52.14	7.38	24.87	57.89	4.62	6.85
sab03-13-7	17.48	3.37	0.25	−0.91	0.08	11.49	1.38	0.62	0.02	37.88	7.38	18.71	57.89	2.76	6.85
sab03-14b-1	17.47	2.69	0.44	−1.11	0.13	9.90	0.53	0.57	0.03	147.60	42.33	103.27	42.03	14.32	3.34
sab03-14b-2	17.47	2.23	0.44	−1.23	0.13	9.60	0.53	0.56	0.03	161.35	42.33	138.07	42.03	8.32	3.34
sab03-14b-3	17.47	na		na		8.32	0.53	0.56	0.03	141.18	42.33	140.35	42.03	17.39	3.34
sab03-14b-4	17.47	2.61	0.44	−1.33	0.13	9.58	0.53	0.55	0.03	183.82	42.33	186.26	42.03	11.85	3.34
sab03-14c-2	17.47	3.10	0.44	−1.01	0.13	8.50	0.53	0.62	0.03	78.79	42.33	44.85	42.03	16.15	3.34
sab03-14c-3	17.47	3.50	0.44	−0.97	0.13	9.22	0.53	0.62	0.03	49.01	42.33	70.88	42.03	7.47	3.34
sab03-15a	17.37	3.87		−0.68		5.43		0.56		24.46		50.23		6.63	
sab03-15b	17.37	3.70		−0.78		7.40		0.52		41.09		259.70		23.44	
SAB03-16A-C	16.96	2.99		−0.83		12.32		0.57		118.65		152.04		16.62	
SAB03-16AD	16.96	3.19		−0.68		6.88		0.56		53.96		119.62		12.67	
SAB03-16B-C	16.96	3.61		−0.65		7.70		0.55		53.49		86.38		7.61	
SAB03-16B-D	16.96	3.35		−0.89		8.22		0.54		122.72		63.48		16.02	
(B) Geochemical data from oyster *Liostrea hisingeri* — altered															
SAB03-1	20.92	−2.65		−5.58		13.63		0.25		1255.98		34.60		25.25	
SAB03-16B-1	16.96	3.37		−0.54		12.28		0.16		1039.88		1075.76		9.07	
sab03-17	16.72	−2.40		−8.69		19.04		0.76		781.53		3062.68		207.01	
SAB03-8B	18.13	3.03		0.68		12.51		0.45		424.34		141.31		67.23	
SAB03-16B-2	16.96	3.22		−0.81		9.61		0.48		310.82		50.99		17.40	
sab03-7-4	18.55					12.69		0.61		155.21		1290.27		302.88	
sab03-14c-1	17.47	3.40		−0.63		8.52		0.60		47.98		209.41		175.97	
sab03-14c-4	17.47	3.17		−1.47		15.17		0.60		41.93		116.78		92.64	
sab03-12	17.56					12.79		0.56		117.04		167.07		80.49	

		%se		%se		%se
Shell 14a		2.5		10.7		3	0.3
Shell 16b	4	2.8		18.5		8.2	0.5
Level 14	4	8.9		9		4.8	3.1
Level 16	3	4.4		5.3		5.4	1.1
Level 10/11	3	no data		no data		6.6	0.7

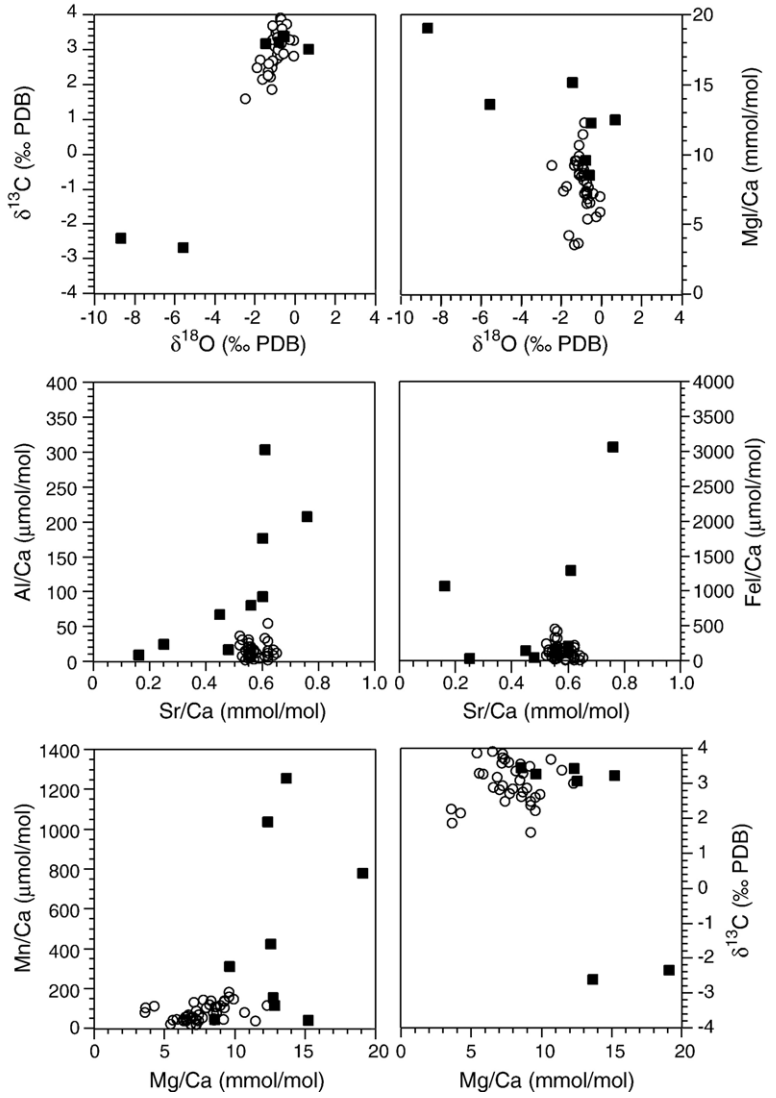

Fig. 4. Cross plots for geochemical data from oyster low-Mg calcite. Black squares in all plots indicate altered oyster data. White circles are data from unaltered oyster calcite. Note the clearly offset values for the rejected oyster data and the uncorrelated values for the unaltered oysters.

priscum show sporadic spikes during the Rhaetian (Courtinat and Piriou, 2002). Organic geochemical analyses of Rhaetian sediments by Thomas et al. (1993) show the presence of abundant dinosteranes, which could be evidence that dinoflagellate cysts form an important part of amorphous organic matter (AOM), indicating the potential shortcomings of a cyst-record only. However, interpreting these previous reports is complicated, because published records of acritarch and prasinophyte abundance and diversity for the Late Triassic to Early Jurassic are generally mostly qualitative (e.g. Beutler et al., 1996; Courtinat et al., 1998; Lund, 2003). The Early Jurassic acritarch microflora, with *Micrhystridium fragile* as the dominant species (Cole and Harding, 1998), shows a general decrease in abundance but a gradual increase in diversity after the T–J boundary, reaching a zenith in the earliest Late Pliensbachian (Wall, 1965; Van de Schootbrugge et al., 2005). Therefore, the sharp increase in both acritarch and prasinophyte species diversity and abundance close to the T–J boundary is an exceptional feature that deserves further consideration against the backdrop of global extinction scenarios.

4.2. Phytoplankton response to the T–J environmental perturbation

Based on the micropalaeontological record, export production in Palaeozoic oceans appears to have been

Table 3
Comparison of geochemical data obtained from fossil and extant oysters

Source	Specimens analysed	Sr	Mg	Fe	Mn
		ppm	ppm	ppm	ppm
This study	Range of well preserved data	457 – 575	863 – 2957	10 – 261	10 – 101
Almeida et al. (1998)	*Crassostrea gigas from estuary mouth*	545 – 759	1300 – 2100	23 – 146	6 – 12
Morrison and Brand (1986)	Low-Mg Calcite bivalves.	250 – 2500	1000 – 10000	8 – 1000	1– 150
Stenzel (1971)	Modern oyster *Crassostrea virginica*	404 – 760	~ 2000	~ 900	~ 100

dominated by phytoplankton belonging to green algal classes, such as the Prasinophyceae (Chlorophyta) and the acritarchs (meaning of uncertain affinity). Although many acritarchs generally resemble dinoflagellates in shape and form, they lack distinctive dinoflagellate characteristics, such as a plate-like pattern on the cyst-wall (paratabulation) or a clearly defined excystment opening (archeopyle), and hence are not formally classified as dinoflagellates. The ultrastructure and organic geochemical composition of some Neoproterozoic acritarchs have been directly linked to Chlorophyceae, a clade of green algae closely related to Prasinophyceae (Al-Arouri et al., 1999).

Green algae typically have chlorophyll *a* and *b* in their photosynthetic organelles, producing a green colour. The diversity of both acritarchs and prasinophytes reached a zenith during the Ordovician to Early Devonian and declined sharply from the Late Devonian to Carboniferous. By Permian times, acritarch and prasinophyte diversity had reached an all time low, but it remains unclear which groups took their place during the Triassic. Dinoflagellates and coccolithophorids, two groups of 'red' phytoplankton (characterized by chlorophyll *a* and *c* in their chloroplasts and producing a red colour) that would come to dominate Mesozoic marine micropalaeontological records (Falkowski et al., 2004), did not rise to prominence until the Jurassic (Fig. 5).

The success of green algal phytoplankton during the Palaeozoic has been ascribed to sluggish ocean circulation and consequent nutrient starvation of the photic zone (Martin, 1996). However, other environmental controls, such as irradiance, salinity and temperature, and which may have been important in the selection of both acritarchs and prasinophytes, are poorly understood and cannot easily be constrained empirically from extant taxa. Carbon isotope analyses of single specimens of the Proterozoic acritarch *Dictyosphaera delicata* indicate that these early eukaryotes thrived under exceptionally high pCO_2 (Kaufman and Xiao, 2003) ranging from 10 to 200 times present atmospheric levels (~3600–70,000 μatm CO_2). The long-term diversity of acritarchs appears to correlate closely with pCO_2 reconstructions for the Phanerozoic (Berner, 1991; Fig. 5). Acritarchs and prasinophytes rose to prominence during the Early Palaeozic in conjunction with elevated pCO_2. However, their importance declined as genus and species numbers crashed following a major decrease in pCO_2 levels during the late Devonian and Carboniferous (Downie, 1966; Tappan, 1980). Our results from St Audrie's Bay indicate that blooms of acritarchs and prasinophytes occurred in relation to the postulated increase in pCO_2, during the main C-isotope anomaly (Hesselbo et al., 2002, 2004).

Prasinophytes have been regarded as 'disaster species' because they appear to prefer special environmental conditions and are generally more abundant when other phytoplankton taxa are absent (Tappan, 1980). Although this designation certainly does not work for the Palaeozoic, during which they were an important group of primary producers, such an epithet is more appropriate for the Mesozoic for which prolific assemblages of acritarchs and prasinophytes are generally rare (Falkowski et al., 2004). The Toarcian Oceanic Anoxic Event (Prauss and Riegel, 1989; Prauss et al., 1991; Van de Schootbrugge et al., 2005), which has been linked to elevated pCO_2, global warming and increased surface water stratification induc-

Table 4
Concentrations of trace metals within individual oyster shells along transects from the umbo to the shell margin

	$\delta^{13}C$	$\delta^{18}O$	Mg	Sr	Mn	Fe	Al
	‰	‰	ppm	ppm	ppm	ppm	ppm
SHELL 1							
Umbo	2.7	−1.7	1866	489	80	246	3.0
	2.8	−0.9	2082	490	59	126	2.2
	2.9	−0.9	1738	480	49	108	4.5
	2.9	−0.9	2156	489	64	191	2.4
	2.8	−0.7	1920	490	59	127	3.7
	2.6	−1.1	2065	480	61	261	7.4
	2.5	−1.2	2214	486	76	193	7.2
Margin	2.4	−1.4	2217	486	78	261	8.6
SHELL 2							
Umbo	3.3	−1.1	2086	489	43	59	2.4
	3.6	−0.9	2049	500	28	79	0.9
	3.7	−0.4	1737	495	14	74	2.2
Margin	3.7	−1.1	2573	493	46	117	5.8

Concentrations in ppm were converted from Element/Calcium molar ratios by first calculating weight ratios then assuming the calcite to be 40% calcium by weight.

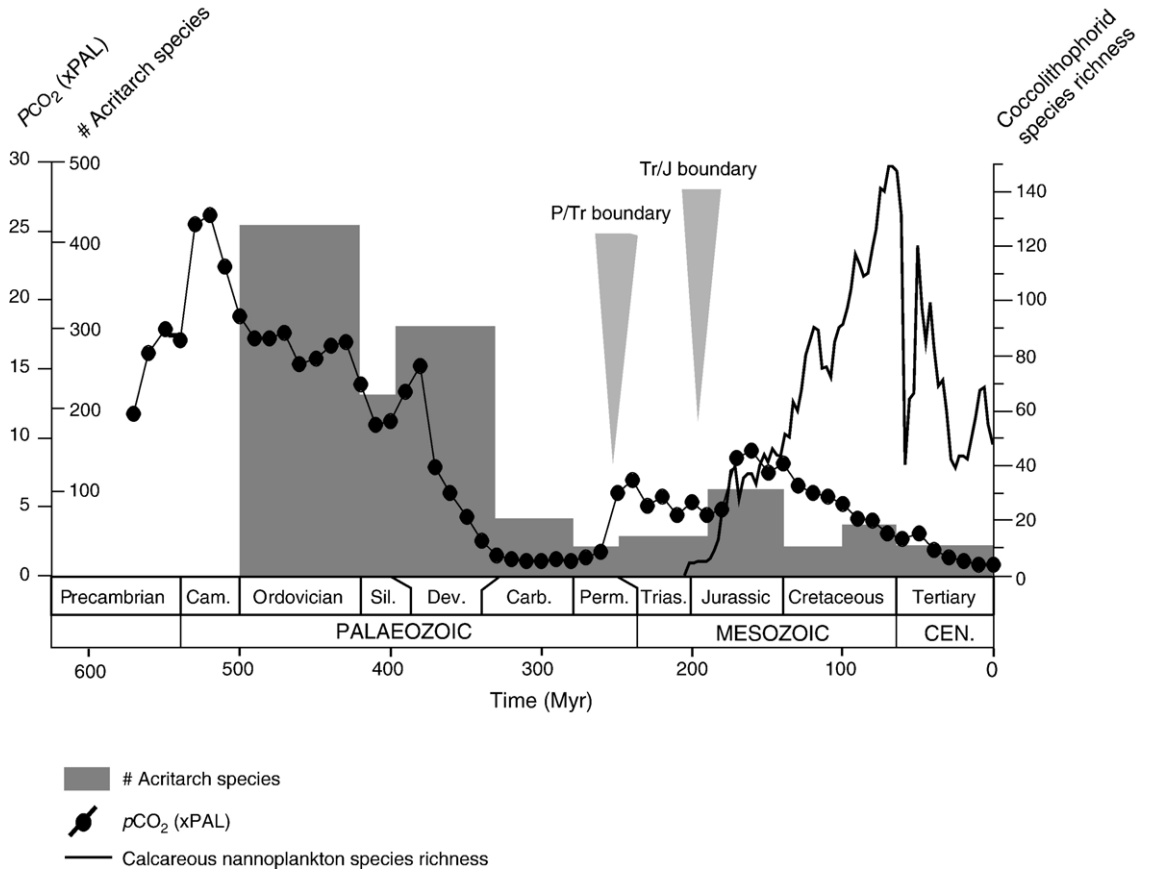

Fig. 5. Diagram showing correlation between number of acritarch species (after Tappan, 1980), pCO_2 during the Phanerozoic (modified from Berner, 1991) and species richness of calcareous nannofossils for the Mesozoic and Cenozoic (after Bown et al., 2004).

ing anoxic conditions (Küspert, 1982; Jenkyns, 1988), appears to be the exception to the rule.

A rapid increase in Late Triassic pCO_2, would lead to acidification of surface waters (i.e. lowering pH), and inhibit calcification. Indeed, coccolithophorids suffered a major set back across the T–J boundary; 2 out of 3 freshly evolved genera (and 4 out 5 species) went extinct during the Late Triassic (Bown, 1998; Bown et al., 2004). The murolith, *Crucirhabdus primulus,* is the only taxon that survived the terminal Triassic extinction, and its ecological preferences remain unclear. The ensuing diversification of calcareous nannoplankton during the Mesozoic may in part be related to lower pCO_2 levels relative to those of the Palaeozoic (Fig. 5). Several studies have highlighted the interactions between carbon dioxide levels (anthropogenic or natural) and calcification in marine zoo-and phytoplankton (Riebesell et al., 2001; Feely et al., 2004). Culture experiments on living calcareous phytoplankton nannofloral assemblages have clearly indicated that higher levels of carbon dioxide hamper biocalcification and can trigger "malformation" and drastic reductions in $CaCO_3$ production rates (Riebesell et al., 2001).

The nannolith *Schizosphaerella punctulata* (incertae sedis) has been interpreted as a calcareous dinoflagellate cyst due to its cyst-like ultrastructure and its high abundance in epicontinental seas (Kälin and Bernoulli, 1984). At first sight, the presence of *S. punctulata* seems to contradict the bio-calcification crisis that occurred across the T–J boundary. However, *S. punctulata* is extremely rare during this time interval and observed specimens appear to be much smaller than their Jurassic successors. The average change in minor diameter from 10 μm to 6.7 μm could indicate under-calcified specimens. It is worth mentioning that *S. punctulata* experienced a major crisis prior to the highly eutrophic Toarcian OAE (Erba, 2004; Tremolada et al., 2005). As a consequence, high abundances of *S. punctulata* in Early Jurassic carbonates have been interpreted as indicative of oligotrophic conditions or a deep nutricline (Mattioli, 1997; Mattioli

and Pittet, 2004). In this respect it is interesting to note that dwarfism was also observed for planktonic foraminifera in the aftermath of the end-Cretaceous mass-extinction (Abramovich and Keller, 2003).

Was elevated carbon dioxide pressure in the atmosphere and the surface ocean the sole reason for triggering blooms of organic-walled phytoplankton? What can we learn from our oyster data about temperature and salinity changes that affected phytoplankton assemblages across the T–J boundary? Because the oxygen isotope composition of Triassic seawater (δ_w) is unknown, it is not possible to derive absolute palaeotemperature from $\delta^{18}O_{oyster}$ using the typical palaeotemperature equation from Hudson and Anderson (1989). However, based on an approximate 0.25‰ $\delta^{18}O$ change per 1 °C temperature change, we calculate a ΔT of 10 °C during the acritarch bloom. An 80% increase in Mg/Ca ratios (from 5 mmol mol^{-1} to 9 mmol mol^{-1}) amounts to a temperature increase of about 8 °C using the benthic foraminiferal Mg/Ca-temperature calibration of 1 °C per 10% increase (Rosenthal et al., 1997; Lear et al., 2002; Bailey et al., 2003).

These temperature changes exceed the estimates from carbon cycle modeling (Beerling and Berner, 2002), which range from 2–4 °C. Analyses of gastropod shells suggest that Sr/Ca ratios in *Conus* sp. are better correlated with temperature than Mg/Ca ratios, which may also be influenced by salinity and vital effects (Gentry et al., 2004). The results of that study suggest an exponential Sr/Ca increase of ~6% per 1 °C. Using this dependence for our oyster data, the 0.12 mmol mol^{-1} increase in Sr/Ca translates to ~4 °C temperature change. We ascribe the residual change in oxygen isotope values (~1.5‰) to a decrease in salinity of 3PSU, which is a relative change in water mass conditions most likely related to increased freshwater runoff.

Salinity is thought to be a critical factor in acritarch palaeoecology and may also exert influence on the morphology of certain species, especially on the length of spines (Servais et al., 2004). A decrease in surface water salinity across the T–J boundary is compatible with a scenario of increased carbon dioxide levels and greenhouse warming, causing increased run-off and stratification of shallow marine environments. The effects of a 2- to 8-fold increase in carbon dioxide were modelled by Huynh and Poulsen (2005) to have led to severe salinity stratification as a result of high run-off and decreased equator to pole temperature-gradients during the Late Triassic. Their model also predicts the development of widespread anoxia, implicated in the marine mass-extinction by Hallam and Wignall (1997b).

4.3. The T–J boundary event in the light of past and present environmental changes

In the contemporary world, there are serious concerns about the potential impact of anthropogenic CO_2 emissions on the saturation state of the global oceans (Feely et al., 2004) and the consequences for calcifying organisms, such as corals (Kleypas et al., 1999), coccolithophorids (Riebesell et al., 2001), and foraminifera (Barker and Elderfield, 2002). The surface ocean today acts as a sink for as much as half of excess CO_2 expelled by fossil fuel burning, resulting in a decrease in $[CO_3^{2-}]$, and hence a lowered potential for calcifying organisms to secrete their $CaCO_3$ skeletons. Anthropogenic perturbation of the global carbon cycle almost certainly will change the ecological balance in favor of non-calcifying organisms within this century (Sabine et al., 2004). The estimated $\sim 2.6 * 10^{10}$ kg CO_2 yr^{-1} (assuming a 500 ka interval for the magmatic event, Olsen et al., 1996; Knight et al., 2004) emission rates of CO_2 from the CAMP were, by comparison, extremely small relative to the emission of $1 * 10^{13}$ kg CO_2 yr^{-1} from anthropogenic sources. If the end-Triassic degassing of continental flood basalts was directly implicated in causing a shift from calcareous phytoplankton to organic-walled phytoplankton, our results suggest that future greenhouse gas emissions could set the stage for chlorophytes to rise to prominence once again.

Our results and analysis allow parallels to be drawn between the T–J mass-extinction event and the one that marked the P–T boundary. The end-Permian extinction coincides with globally identified negative C-isotope excursions in carbonates and organic matter (e.g. Magaritz et al., 1992; Sephton et al., 2002), an extensive biocalcification crisis (Payne et al., 2004) including the extinction of all tabulate and rugose corals and causing a global reef gap (Scrutton, 1988; Stanley, 2001), and voluminous continental flood basalt outflow in the Siberian Traps (Renne et al., 1995). In addition, the P–T boundary is marked by a global abundance of acritarchs of the *Micrhystridium–Veryhachium* plexus (e.g. Eshet et al., 1995). Interestingly, *Micrhystridium microspinosum*, the taxon that occurs so prominently in T–J boundary beds of the St Audrie's Bay section, has previously been reported from P–T boundary beds in Pakistan (Sarjeant, 1970; Sarjeant, 1973). Blooms of acritarchs and prasinophytes have also been reported from anoxic Early Triassic age sediments from Greenland (Twitchett et al., 2001). Although the link between (photic zone?) anoxia and green algal phytoplankton blooms remains to be explored in more detail, we suggest that blooms of prasinophytes and acritarchs are symptomatic for elevated pCO_2 and

widespread anoxic conditions in shallow marine settings during and after the T–J mass-extinction event.

5. Conclusions

The T–J boundary, recorded in the St Audrie's Bay section, clearly suggests a marked disruption in the evolution of modern eukaryotic phytoplankton taxa. Members of the red-lineage, i.e. dinoflagellates and coccolithophorids, which had only just originated during the Carnian–Norian, appear to have experienced severe extinction. Only two, unequivocal, cyst-producing dinoflagellate genera are known from the earliest Jurassic (*Dapcodinium* and *Beaumontella*) and only one Late Triassic calcareous nannoplankton taxa survived into the Early Jurassic (*Crucirhabdus primulus*). The absence of these taxa or their closely related derivatives across the boundary appears to have been ecologically exploited by members of the green algal line, such as prasinophytes and acritarchs, which dominated primary production during most of the Palaeozoic, but had been in steady decline since the Late Palaeozoic. Prasinophytes, but also acritarchs, may thus be typified as 'disaster species'. Their response resembles that of such mass-occurrences after the P–T boundary, which may be important in elucidating causes for both mass-extinction events. Our St Audrie's Bay geochemical records obtained from the oyster *Liostrea hisingeri* indicate that water masses that flooded the Blue Lias shores of the London–Brabant Massif during the Hettangian warmed by 4 °C and decreased in salinity by at least 3 PSU, creating conditions that were prone to stratification and the development of anoxia.

Many factors control the distribution of phytoplankton in the oceans today. Our analysis shows that on very long time scales the diversity of acritarchs and prasinophytes may have been governed by pCO_2 of the atmosphere and hence of the upper ocean. CO_2 also plays a crucial role in the calcification of calcareous organisms. Rapid and large increases in pCO_2 may temporarily acidify the upper ocean, thereby causing problems for calcareous organisms, such as foraminifera, coccolithophorids, bivalves and corals. It may thus be hypothesized that the rapid addition of volcanic CO_2 from the Central Atlantic Magmatic Province at the Triassic–Jurassic boundary led to a shut-down of calcification, allowing non-calcareous phytoplankton, especially those that were adapted to extremely high pCO_2, to proliferate. Members of the red-lineage did not recover until the Late Pliensbachian, when both dinoflagellates and coccolithophorids rapidly diversified. About the same time scleractinian reefs recovered along the southern margin of the Tethys. If our scenario is correct it took almost 8 million years to put all the excess CO_2 back into the deep ocean and/or the sedimentary reservoir, testifying to the dramatic changes that took place at the Triassic–Jurassic boundary.

Acknowledgements

This study was supported by the National Science Foundation (NSF) Biocomplexity grant OCE-0084032 (Evolution and Radiation of Eukaryotic Phytoplankton Taxa-EREUPT) to Paul G. Falkowski. The authors thank Jonah Chitoli for the excellent work he did processing our samples for palynomorphs at the Natural History Museum in London. Jim Wright at Rutgers University is thanked for his help with the stable isotope data. Thoughtful and valuable comments by John Marshall, Stephen Hesselbo and an anonymous reviewer helped to strengthen the contents of this contribution.

References

Al-Arouri, K., Greenwood, P.F., Walter, M., 1999. A possible chlorophycean affinity of some Neoproterozoic acritarchs. Org. Geochem. 30, 1323–1337.

Abramovich, S., Keller, G., 2003. Planktonic foraminiferal response to the latest Maastrichtian abrupt warm event: a case study from South Atlantic DSDP Site 525A. Mar. Micropaleontol. 48, 225–249.

Almeida, M.J., Machado, J., Moura, G., Azevedo, M., Coimbra, J., 1998. Temporal and local variations in the biochemical composition of *Crassostrea gigas* shells. J. Sea Res. 40, 233–249.

Bailey, T.R., Rosenthal, Y., McArthur, J.M., van de Schootbrugge, B., Thirlwall, M.F., 2003. Paleoceanographic changes of the Late Pliensbachian–Early Toarcian interval: a possible link to the genesis of an Oceanic Anoxic Event. Earth Planet. Sci. Lett. 212, 307–320.

Barker, S., Elderfield, H., 2002. Foraminiferal calcification response to glacial–interglacial changes in atmospheric CO_2. Science 297, 833–836.

Barker, S., Greaves, M., Elderfield, H., 2003. A study of cleaning procedures used for foraminiferal Mg/Ca paleothermometry. Geochem., Geophys., Geosyst. 4, 8407.

Beerling, D.J., Berner, R.A., 2002. Biogeochemical constraints on the Triassic–Jurassic boundary carbon cycle event. Glob. Biogeochem. Cycles 16, 101–113.

Berner, R.A., 1991. A model for atmospheric CO_2 over Phanerozoic time. Am. J. Sci. 291, 339–376.

Beutler, G., Heunisch, C., Luppold, F.W., Rettig, B., Röhling, H.-G., 1996. Muschelkalk, Keuper und Lias am Mittellandkanal bei Sehnde (Niedersachsen) und die regionale Stellung des Keupers. Geol. Jahrb. 145, 67–197.

Bown, P.R., 1998. Triassic. In: Bown, P.R. (Ed.), Calcareous Nannofossil Biostratigraphy. Kluwer, Dordrecht, pp. 29–32.

Bown, P.R., Young, J.R., 1998. Techniques. In: Bown, P.R. (Ed.), Calcareous Nannofossil Biostratigraphy. Kluwer, Dordrecht, pp. 16–28.

Bown, P.R., Lees, J.A., Young, J.R., 2004. Calcareous nannoplankton evolution and diversity through time. In: Young, J.R., Thierstein, H. (Eds.), Coccolithophorids: From Molecular Processes to Global Impact. Elsevier, pp. 481–508.

Brand, U., Veizer, J., 1980. Chemical diagenesis of a multicomponent carbonate system — I: trace elements. J. Sediment. Petrol. 50, 1219–1236.

Cole, D.C., Harding, I.C., 1998. Sequence palynology in the Wessex Basin: the Lower Jurassic strata (Sinemurian to Pliensbachian stages) of the Dorset Coast, England. In: Underhill, J. (Ed.), Development and Evolution of the Wessex Basin. Geological Society of London, Special Publication, vol. 133, pp. 165–187.

Cohen, A.S., Coe, A.L., 2002. New geochemical evidence for the onset of volcanism in the Central Atlantic Magmatic Province and environmental change at the Triassic–Jurassic boundary. Geology 30, 267–270.

Courtinat, B., Piriou, S., 2002. Palaeoenvironmental distribution of the Rhaetian dinoflagellate cysts Dapcodinium priscum Evitt 1961 emend. Below 1987 and Rhaetogonyaulax rhaetica (Sarjeant) Loeblich and Loeblich 1976 emend. Harland et al. 1975 emend. Below 1987. Geobios 35, 429–439.

Courtinat, B., Malartre, F., Giraud, F., 1998. Le Rhetien en region Lyonnaise: analyse palynologique. Geol. Fr. 1, 3–19.

Downie, C., 1966. The geological history of the microplankton. Rev. Palaeobot. Palynol. 1, 269–281.

Erba, E., 2004. Calcareous nannofossils and Mesozoic oceanic anoxia. Mar. Micropaleontol. 52, 85–106.

Eshet, Y., Rampino, M.R., Visscher, H., 1995. Fungal event and palynological record of ecological crisis and recovery across the Permian–Triassic boundary. Geology 23, 967–970.

Falkowski, P.G., Schofield, O., Katz, M.E., van de Schootbrugge, B., Knoll, A.H., 2004. Why is the land green and the ocean red? In: Thierstein, H., Young, J.R. (Eds.), Coccolithophores: From Molecular Processes to Global Impact. Elsevier, pp. 429–453.

Feely, R.A., Sabine, C.L., Lee, K., Berelson, W., Kleypas, J., Fabry, V. J., Millero, F.J., 2004. Impact of anthropogenic CO_2 on the $CaCO_3$ system in the oceans. Science 305, 362–366.

Galli, M.T., Jadoul, F., Bernasconi, S.M., Weissert, H., 2005. Anomalies in global carbon cycling and extinction at the Triassic/Jurassic boundary: evidence from a marine C-isotope record. Palaeogeogr. Palaeoclim. Palaeoecol. 216, 203–214.

Gentry, K., Sosdian, S., Grossman, E.L., Lear, C., Rosenthal, Y., 2004. Paleoenvironmental reconstructions using seasonal isotope and trace-metal profiles of serially-sampled gastropods. AGU Fall Meeting.

Guex, J., Bartolini, A., Atudorei, V., Taylor, D., 2003. Two negative $\delta^{13}C_{org}$ excursions near the Triassic–Jurassic boundary in the New York Canyon area (Gabbs Valley Range, Nevada). Bull. Geol. Lausanne 360, 1–4.

Guex, J., Bartolini, A., Atudorei, V., Taylor, D., 2004. High-resolution ammonite and carbon isotope stratigraphy across the Triassic–Jurassic boundary at New York Canyon (Nevada). Earth Planet. Sci. Lett. 225, 29–41.

Hallam, A., 1994. Strontium isotope profiles of Triassic–Jurassic boundary sections in England and Austria. Geology 22, 1079–1082.

Hallam, A., 1997. Estimates of the amount and rate of sea-level change across the Rhaetian–Hettangian and Pliensbachian–Toarcian boundaries (latest Triassic to early Jurassic). J. Geol. Soc. (Lond.) 154, 773–779.

Hallam, A., Wignall, P.B., 1997a. Mass extinction and sea level-change. Earth-Sci. Rev. 48, 217–258.

Hallam, A., Wignall, P.B., 1997b. Mass-Extinctions and their Aftermath. Oxford University Press, Oxford, p. 320.

Hamilton, G., 1982. Triassic and Jurassic calcareous nannofossils. In: Lord, A.R. (Ed.), A Stratigraphical Index of Calcareous Nannofossils. Ellis Horwood, Chichester, pp. 17–39.

Hautmann, M., 2004. Effect of end-Triassic CO_2 maximum on carbonate sedimentation and marine mass-extinction. Facies 50, 257–261.

Hesselbo, S.P., Robinson, S.A., Surlyk, F., Piasecki, S., 2002. Terrestrial and marine extinction at the Triassic–Jurassic boundary synchronized with major carbon cycle perturbation: a link to initiation of massive volcanism. Geology 30, 251–254.

Hesselbo, S.P., Robinson, S.A., Surlyk, F., 2004. Sea level change and facies development across potential Triassic–Jurassic boundary horizons, SW Britain. J. Geol. Soc. (Lond.) 161, 365–379.

Hounslow, M.W., Posen, P.E., Warrington, G., 2004. Magnetostratigraphy and biostratigraphy of the Upper Triassic and lowermost Jurassic succession, St Audrie's Bay, UK. Palaeogeogr. Palaeoclimatol. Palaeoecol. 213, 331–358.

Hudson, J.D., Anderson, T.F., 1989. Ocean temperatures and isotopic compositions through time. Trans. R. Soc. Edinb. Earth Sci. 80, 183–192.

Huynh, T.T., Poulsen, C.J., 2005. Rising atmospheric CO_2 as a possible trigger for the end-Triassic mass extinction. Palaeogeogr. Palaeoclimatol. Palaeoecol. 217, 223–242.

Jenkyns, H.C., 1988. The Early Toarcian (Jurassic) anoxic event: stratigraphic, sedimentary, and geochemical evidence. Am. J. Sci. 288, 101–151.

Kälin, O., Bernoulli, D., 1984. Schizosphaerella Deflandre and Dangeard in Jurassic deep water carbonate sediments, Mazagan continental margin (Hole 547B) and Mesozoic Tethys. In: Hinz, K., Winterer, E.L. (Eds.), Init. Rep. Deep Sea Drilling Proj. Leg, vol. 79, pp. 411–435.

Kaufman, A.J., Xiao, S., 2003. High CO_2 levels in the Proterozoic atmosphere estimated from analyses of individual microfossils. Nature 425, 279–282.

Kleypas, J.A., Buddemeier, R.W., Archer, D., Gattuso, J.-P., Langdon, C., Opdyke, B.N., 1999. Geochemical consequences of increased atmospheric carbon dioxide on coral reefs. Science 284, 118–120.

Knight, K.B., Nomade, S., Renne, P.R., Marzoli, A., Bertrand, H., Youbi, N., 2004. The Central Atlantic Magmatic Province at the Triassic–Jurassic boundary: paleomagnetic and 40Ar/39Ar evidence from Morocco for brief, episodic volcanism. Earth Planet. Sci. Lett. 228, 143–160.

Küspert, W., 1982. Environmental change during oil shale deposition as deduced from stable isotope ratios. In: Einsele, S., Seilacher, A. (Eds.), Cyclic and Event Stratification. Springer–Verlag, Berlin, Germany, pp. 482–501.

Lear, C.H., Rosenthal, Y., Slowey, N., 2002. Benthic foraminiferal Mg/Ca paleothermometry: a revised core-top calibration. Geochim. Cosmochim. Acta 66, 3375–3387.

Lund, J.J., 2003. Rhaetian to Pliensbachian palynostratigraphy of the central part of the NW German Basin exemplified by the Eitzendorf 8 well. Cour. Forsch.-InSt Senckenberg 241, 69–83.

Martin, R.E., 1996. Secular increase in nutrient levels through the Phanerozoic: implications for productivity, biomass, and diversity of the marine biosphere. Palaios 11, 209–219.

Magaritz, M., Krishnamurthy, R.V., Holser, W.T., 1992. On the parallel trends in carbon isotopes of organic and inorganic carbon reservoirs across the Permian/Triassic boundary. Am. J. Sci. 292, 727–739.

Marzoli, A., Renne, P.R., Piccirillo, E.M., Ernesto, A., Bellieni, G., De Min, A., 1999. Extensive 200-million-year-old continental flood basalts of the central Atlantic magmatic province. Science 284, 616–618.

Mattioli, E., 1997. Nannoplankton productivity and diagenesis in the rhythmically bedded Toarcian–Aalenian Fiuminata section (Umbrian–Marche Apennine, central Italy). Palaeogeogr. Palaeoclimatol. Palaeoecol. 130, 113–133.

Mattioli, E., Pittet, B., 2004. Spatial and temporal distribution of calcareous nannofossils along a proximal–distal transect in the Lower Jurassic of the Umbria–Marche Basin (central Italy): Palaeogeogr. Palaeogeogr. Palaeoclimatol. Palaeoecol. 205, 295–316.

McElwain, J.C., Beerling, D.J., Woodward, F.I., 1999. Fossil plants and global warming at the Triassic–Jurassic boundary. Science 285, 1386–1390.

Morrison, J.O., Brand, U., 1986. Geochemistry of recent marine invertebrates. Geosci. Can. 13 (4), 237–254.

Newell, N.D., 1963. Crises in the history of life. Sci. Am. 208, 76–92.

Olsen, P.E., Schlische, R.W., Fedosh, M.S., 1996. 580 Ky duration of the Early Jurassic flood basalt event in eastern North America estimated using Milankovitch cyclostratigraphy. In: Morales, M. (Ed.), The Continental Jurassic. Museum of Northern Arizona Bull., vol. 60, pp. 11–22.

Olsen, P.E., Kent, D.V., Sues, H.-D., Koeberl, C., Huber, H., Montanari, A., Rainforth, E.C., Fowell, S.J., Szajina, M.J., Hartline, B., 2002. Ascent of dinosaurs linked to an iridium anomaly at the Triassic–Jurassic boundary. Science 296, 1305–1307.

Orbell, G., 1973. Palynology of the British Rhaeto–Liassic. Bull. Geol. Surv. G. B. 44, 1–44.

Payne, J.L., Lehrmann, D.J., Wei, J., Orchard, M.J., Schrag, D.P., Knoll, A.H., 2004. Large perturbations of the carbon cycle during recovery from the end-Permian extinction. Science 305, 506–509.

Prauss, M., Riegel, W., 1989. Evidence of phytoplankton associations for causes of black shale formation in epicontinental seas. Neues Jahrb. Geol. Palaontol., Monatsh. 11, 671–682.

Prauss, M., Ligouis, B., Luterbacher, H., 1991. Organic matter and palynomorphs in the 'Posidonienschiefer' (Toarcian, Lower Jurassic) of southern Germany. In: Tyson, R.V., Pearson, T.H. (Eds.), Modern and Ancient Continental Shelf Anoxia. Geological Society, London, pp. 335–352.

Renne, P.R., Zichao, Z., Richards, M.A., Black, M.T., Basu, A.R., 1995. Synchrony and casual relations between Permian–Triassic boundary crises and Siberian flood volcanism. Science 269, 1413–1415.

Riebesell, U., Zondervan, I., Rost, B., Tortell, P.D., Zeebe, R.E., Morel, F.M.M., 2001. Reduced calcification of marine phytoplankton in response to increased atmospheric CO_2. Nature 407, 364–367.

Rosenthal, Y., Boyle, E.A., Slowey, N., 1997. Temperature control on the incorporation of magnesium, strontium, fluorine, and cadmium into benthic foraminiferal shells from Little Bahama Bank: prospects for thermocline paleoceanography. Geochim. Cosmochim. Acta 61, 3633–3643.

Rosenthal, Y., Field, M.P., Sherrell, R.M., 1999. Precise determination of element/calcium ratios in calcareous samples using sector field inductively coupled plasma mass spectrometry. Ann. Chem. 71, 3248–3253.

Sabine, S.L., et al., 2004. The oceanic sink for anthropogenic CO_2. Science 305, 367–371.

Sarjeant, W.A.S., 1970. Acritarchs and Tasmanitids from the Chhidru Formation, Uppermost Permian of West Pakistan. In: Kummel, B., Teichert, C. (Eds.), Stratigraphic Boundary Problems: Permian and Triassic of West Pakistan. Spec. Publ., vol. 4. Department of Geology, University of Kansas, pp. 277–304.

Sarjeant, W.A.S., 1973. Acritarchs and Tasmanitids from the Mianwali and Tredian Formations (Triassic) of the Salt and Surghar Ranges, West Pakistan. In: Logan, A., Hills, L.V. (Eds.), The Permo–Triassic Systems and their Mutual Boundary. Can. Soc. Petrol. Geol., Mem., 2, pp. 35–73.

Scrutton, C.T., 1988. Patterns of extinction and survival in Palaeozoic corals. In: Larwood, G.P. (Ed.), Extinction and Survival in the Fossil Record. Clarendon Press, Oxford, pp. 65–88.

Sephton, M.A., Looy, C.V., Veefkind, R.J., Brinkhuis, H., de Leeuw, J.W., Visscher, H., 2002. A synchronous record of $\delta^{13}C$ shifts in the oceans and atmosphere at the end of the Permian. In: MacLeod, K., Koeberl, C. (Eds.), Catastrophic Events and Mass Extinctions: Impacts and Beyond. Geol. Soc. Am. Spec. Paper, vol. 356, pp. 455–462.

Sepkoski Jr., J.J., 1996. Patterns of Phanerozoic extinction: a perspective from global databases. In: Walliser, O.H. (Ed.), Global Events and Event Stratigraphy in the Phanerozoic. Berlin, Springer, pp. 35–51.

Servais, T., Stricanne, L., Montenari, M., Pross, J., 2004. Population dynamics of galeate acritarchs at the Cambro–Ordovician transition in the Algerian Sahara. Palaeontology 47, 395–414.

Stanley Jr., G.D., 2001. Introduction to reef ecosystems and their evolution. In: Stanley Jr., G.D. (Ed.), The History and Sedimentology of Ancient Reef Systems. Kluwer Academic, New York, pp. 1–36.

Stenzel, H.B., 1971. Oysters. In: Moore, R.C., Teichert, C., Cox, L.R., Newell, N.D. (Eds.), Treatise on Invertebrate Paleontology, Part N: Mollusca 6, Bivalvia (Oysters), vol. 3, pp. 953–1224. University of Kansas, Paleontological Institute and Geological Society of America, Boulder, Colorado, p. 276.

Tanner, L.H., Lucas, S.G., Chapman, M.G., 2004. Assessing the record and causes of Late Triassic extinctions. Earth-Sci. Rev. 65, 103–139.

Tappan, H., 1980. The paleobiology of plant protists. W.H. Freeman and Company, San Francisco, p. 1028.

Thomas, J.B., Marshall, J., Mann, A.L., Summons, R.L., Maxwell, J.R., 1993. Dinosteranes (4,23,24-trimethylsteranes) and other biological markers in dinoglagellate-rich marine sediments of Rhaetian age. Org. Geochem. 20, 91–104.

Tremolada, F., Van de Schootbrugge, B., Erba, E., 2005. The Early Jurassic Schizosphaerellid crisis in Cantabria, Spain: implications for calcification rates and phytoplankton evolution across the Toarcian oceanic anoxic event. Paleoceanography 20, A2011, doi:10.1029/2004PA001120.

Twitchett, R.J., Looy, C.V., Morante, R., Visscher, H., Wignall, P.B., 2001. Rapid and synchronous collapse of marine and terrestrial ecosystems during the end-Permian biotic crisis. Geology 29, 351–354.

Van de Schootbrugge, B., Bailey, T., Rosenthal, Y., Katz, M., Wright, J.D., Feist-Burkhardt, S., Miller, K.G., Falkowski, P.G., 2005. Early Jurassic climate change and the radiation of organic-walled phytoplankton in the Tethys Ocean. Paleobiology 31, 73–97.

Wall, D., 1965. Microplankton, pollen and spores from the Lower Jurassic in Britain. Micropaleontology 11, 151–190.

Ward, P.D., Haggart, J.W., Carter, E.S., Wilbur, D., Tipper, H.W., Evans, T., 2001. Sudden productivity collapse associated with the Triassic–Jurassic boundary mass-extinction. Science 292, 2185–2188.

Ward, P.D., Garrison, G.H., Haggart, J.W., Kring, D.A., Beattie, M.J., 2004. Isotopic evidence bearing on Late Triassic extinction events, Queen Charlotte Islands, British Columbia, and implications for the duration and cause of the Triassic/Jurassic mass extinction. Earth Planet. Sci. Lett. 224, 589–600.

Warrington, G., Cope, J.C.W., Ivimey-Cook, H.C., 1994. St Audrie's Bay, Somerset, England: a candidate Global Stratotype Section and Point for the base of the Jurassic System. Geol. Mag. 133, 191–200.